The Effect of Partial Coherence in Receiving System Noise Temperature on Array Gain for Telemetry and Radio Frequency Carrier Reception for Similar Receiving Systems

M. H. Brockman
Telecommunications Science and Engineering Division

Signal-to-noise ratio improvement realized by arraying receiving systems or stations for coherent reception is reduced when some portion of predetection noise is coherent in the array. This report examines this effect for arrayed receiving systems with essentially equal apertures including presence of a planet in the array beamwidth.

I. Introduction

In earlier reports "Radio Frequency Carrier Arraying for High-Rate Telemetry" (Ref. 1) and "Radio Frequency Carrier Arraying for Near-Maximum Carrier Signal-to-Noise Ratio Improvement" (Ref. 2), the various components of operating system noise temperature (which produce the receiver predetection noise) were treated as statistically independent among the receiving systems of an array. This report considers the effect on predetection signal-to-noise ratio improvement for coherent carrier reception and demodulation for the condition when some portion of the predetection noise is not statistically independent but is coherent among the various receiving systems of the array (for some period of time). The following material is directed toward high-rate telemetry reception with residual radio frequency (RF) carrier. Performance shown herein applies to similar receiving systems with equal predetection noise. A later report will consider the case for unequal predetection noise.

II. Receiver Configuration and Predetection Noise

Figure 1 illustrates a method for achieving RF carrier arraying which provides adequate RF carrier signal-to-noise ratio improvement for high-rate telemetry with residual RF carrier. This configuration was presented in Ref. 1 with a detailed discussion of the received signal as it passes through the receiving systems. Although only two systems are shown in Fig. 1, additional systems can be added to increase the signal-to-noise ratio improvement for high-rate telemetry with residual RF carrier.

Figure 1 can be modified so that much larger antenna separations for the array can be handled conveniently. This modification, described below, represents in general a proposed array configuration for the Mark IV-A DSN system design. In particular, Fig. 1 can be modified so that for receiving system 2, the received signal is down-converted (after the microwave low-noise amplifier) to

an adequately high IF signal frequency that will provide sufficient bandwidth. This down-conversion is accomplished using a stable fixed frequency first local oscillator. The down-converted IF signal is fed over some distance to a mixer located in a central area closely associated with receiving system 1. The local oscillator for this mixer (located in the central area) is effectively the first local oscillator for receiving system 1 down-converted to the appropriate frequency. The resultant output from this mixer (centrally located) is then fed into the IF amplifier (with AGC), shown in Fig. 1. Receiving systems 3 through N are also configured in a manner similar to receiving system 2.

As described in Ref. 1, the predetection noise in each receiving system is measured relative to reference temperature load(s) connected to the low noise amplifier input (during the measurement) and designated as due to the operating equivalent system noise temperature T_{op_1}, T_{op_2}, etc. This predetection noise represents a combination of galactic noise, planetary radiation, atmospheric noise, noise in the antenna sidelobes due to the Earth, noise due to losses in microwave reflectors, and noise due to losses in microwave components all lumped with noise due to the input amplifier(s). The following section will develop an expression for predetection signal-to-noise ratio improvement and the resultant phase noise on the first local oscillator for the case where a portion of the receiver noise is coherent among the various receiving systems of the array. It should be noted that for the results presented in this report, the receiving systems are considered to be similar to each other with essentially equal size antenna apertures and/or equal predetection noise (including the portion which is coherent) for the receiving systems of the array.

III. Predetection Signal-to-Noise Ratio and Resultant Carrier Tracking Loop Phase Noise

With the other receiving system(s) (2 through N) switched out of the summing junction (see Fig. 1), the predetection carrier signal-to-noise power ratio in receiving system 1 is (from Ref. 1)

$$\frac{P_{c1}}{P_{n1}} = \frac{A_1 \cos m_{pD}^2}{NBW_{F_{A1}} N_{o1}} \quad \text{or} \quad \frac{P_{c1}}{NBW_{F_{A1}} N_{o1}} \tag{1}$$

where m_{pd} is the peak phase modulation index and $NBW_{F_{A1}}$ represents the noise bandwidth of the second IF filter F_{A1}. The term N_{o1} is the one-sided noise spectral density for receiver 1 related to T_{op_1} as discussed in the preceding section of this report and in Ref. 1. The receiving system contains a second-order RF carrier phase tracking loop which utilizes a bandpass limiter and a sinusoidal phase detector. The resultant rms phase noise σ_{ϕ_n} at the output of the RF carrier tracking loop (i.e., on the first local oscillator) due to the predetection carrier signal-to-noise ratio within the closed-loop noise bandwidth of the RF carrier tracking loop is (from Ref. 1)

$$\sigma_{\phi_{n1}} = \frac{\frac{N_{o1} \cdot 2B_{L1}}{2}}{P_{c1}} \left[\frac{1 + \frac{P_{c1}}{NBW_{F_{A1}} \cdot N_{o1}}}{0.862 + \frac{P_{c1}}{NBW_{F_{A1}} \cdot N_{o1}}} \cdot \frac{\exp\left(\frac{N_{o1}B_{L1}}{P_{c1}}\right)}{\sinh\left(\frac{N_{o1}B_{L1}}{P_{c1}}\right)} \right]^{1/2} \text{rad, rms} \tag{2}$$

where two-sided closed loop noise bandwidth $2B_{L1}$ can be expressed as

$$2B_{L1} = \frac{2B_{Lo1}}{r_o + 1} \left(1 + r_o \frac{\alpha}{\alpha_{o1}}\right)$$

The term r_o is equal to 2 and α is the bandpass limiter suppression factor (Ref. 1).

Next consider receiving system 2 where a portion of its predetection noise is coherent with a similar portion of the predetection noise in receiving system 1 at the output of the summing junction. Designate ϵ as that portion of the predetection

noise that is coherent, then $1 - \epsilon$ is that portion which is statistically independent. With receiving system 2 connected to the summing junction, the summed carrier predetection signal-to-noise ratio at the output of the summing junction becomes:

$$\frac{P_{c1_{\Sigma 1,2}}}{P_{n1_{\Sigma 1,2}}} = \frac{(A_1 \cos m_{pd} + \beta_2 A_2 \cos m_{pd})^2}{\left[NBW_{F_{A1}} (1 - \epsilon_1) N_{o1} + \beta_2^2 NBW_{F_{A2}} (1 - \epsilon_2) N_{o2}\right] + \left[\left(NBW_{F_{A1}} \cdot \epsilon_1 N_{o1}\right)^{1/2} + \beta_2 \left(NBW_{F_{A2}} \cdot \epsilon_2 N_{o2}\right)^{1/2}\right]^2} \tag{3}$$

For similar systems with essentially equal diameter antennas and aperture efficiencies, and/or equal predetection noise spectral density (including the portion which is coherent), expression (3) can be written as

$$\frac{P_{c1_{\Sigma 1.2}}}{P_{n1_{\Sigma 1.2}}} = \frac{P_{c1}}{NBW_{F_{A1}} \cdot N_{o1}} \cdot \frac{(1 + \beta_2 \gamma_2)^2}{(1 - \epsilon)(1 + \beta_2^2) + \epsilon(1 + \beta_2)^2} \tag{4}$$

where β_2 is the voltage coupling of receiving system 2 relative to receiving system 1 at the output of the summing junction, γ_2^2 is the carrier power-to-noise spectral density ratio of receiving system 2 relative to receiving system 1 and $\epsilon = \epsilon_1 = \epsilon_2$. For N receiving systems arrayed, the predetection carrier signal-to-noise ratio in receiving system 1 is

$$\frac{P_{c1_{\Sigma 1,\ldots,N}}}{P_{n1_{\Sigma 1,\ldots,N}}} = \frac{(A_1 \cos m_{pd} + \beta_2 A_2 \cos m_{pd} + \cdots + \beta_N A_N \cos m_{pd})^2}{\left[NBW_{F_{A1}} (1 - \epsilon_1) N_{o2} + \beta_2^2 NBW_{F_{A2}} (1 - \epsilon_2) N_{o2} + \cdots + \beta_N^2 NBW_{F_{AN}} (1 - \epsilon_N) N_{oN}\right] +}$$

$$\frac{}{\left[\left(NBW_{F_{A1}} \epsilon_1 N_{o1}\right)^{1/2} + \beta_2 \left(NBW_{F_{A2}} \epsilon_2 N_{oN}\right)^{1/2} + \cdots + \beta_N \left(NBW_{F_{AN}} \epsilon_N N_{oN}\right)^{1/2}\right]^2} \tag{5}$$

For similar systems (as described above for expression 3), expression (5) becomes

$$\frac{P_{c1_{\Sigma 1,\ldots,N}}}{P_{n1_{\Sigma 1,\ldots,N}}} = \frac{P_{c1}}{NBW_{F_{A1}} \cdot N_{o1}} \cdot \frac{(1 + \beta_2 \gamma_2 + \cdots + \beta_N \gamma_N)^2}{(1 - \epsilon)(1 + \beta_2^2 + \cdots + \beta_N^2) + \epsilon (1 + \beta_2 + \cdots + \beta_N)^2} \tag{6}$$

The resultant rms phase noise ($\sigma_{\phi_{n1\Sigma 1,2}}$) at the output of the RF carrier tracking loop (i.e., on the first local oscillator signal) in receiving system 1 due to the predetection signal-to-noise ratio within the closed-loop noise bandwidth of the RF carrier tracking loop becomes

$$\sigma_{\phi_{n1\Sigma 1,2}} = \frac{\frac{N_{o1}}{2} \cdot 2B_{L1}}{P_{c1}} \cdot \frac{1}{\eta_2'} \left[\frac{1 + \frac{P_{c1}\eta_2'}{NBW_{F_{A1}} \cdot N_{o1}}}{0.862 + \frac{P_{c1} \cdot \eta_2'}{NBW_{F_{A1}} \cdot N_{o1}}} \cdot \frac{\exp\left(\frac{N_{o1} \cdot B_{L1}}{P_{c1} \cdot \eta_2'}\right)}{\sinh\left(\frac{N_{o1} \cdot B_{L1}}{P_{c1} \cdot \eta_2'}\right)}\right]^{1/2} \text{rad, rms} \tag{7}$$

where

$$\eta_2' = \frac{(1 + \beta_2 \gamma_2)^2}{(1 - \epsilon)(1 + \beta_2^2) + \epsilon(1 + \beta_2)^2} \tag{7a}$$

for two similar receiving systems arrayed. For N similar receiving systems arrayed, the resultant rms phase noise ($\sigma_{\phi_{n1\Sigma 1,\ldots,N}}$) becomes

$$\sigma_{\phi_{n1\Sigma 1,\ldots,N}} = \frac{\frac{N_{oN}}{2} \cdot 2B_{L1}}{P_{c1}} \cdot \frac{1}{\eta'_N} \left[\frac{1 + \frac{P_{c1} \cdot \eta'_N}{NBW_{F_{A1}} \cdot N_{o1}}}{0.862 + \frac{P_{c1} \cdot \eta'_N}{NBW_{F_{A1}} \cdot N_{o1}}} \cdot \frac{\exp\left(\frac{N_{o1} \cdot B_{L1}}{P_{c1} \cdot \eta'_N}\right)}{\sinh\left(\frac{N_{o1} \cdot B_{L1}}{P_{c1} \cdot \eta'_N}\right)} \right]^{1/2} \text{rad, rms} \tag{8}$$

where

$$\eta'_N = \frac{(1 + \beta_2\gamma_2 + \cdots + \beta_N\gamma_N)^2}{(1 - \epsilon)(1 + \beta_2^2 + \cdots + \beta_N^2) + \epsilon(1 + \beta_2 + \cdots + \beta_N)^2} \tag{8a}$$

The discussion above has addressed predetection carrier signal-to-noise ratio improvement and resultant phase noise. It should be noted that for the condition where the varying group delay on the telemetry sidebands is tracked out among the various receiving systems of the array (which is accomplished at baseband for the configuration shown in Fig. 1), the improvement in telemetry signal-to-noise ratio is also represented by expressions (7a) and (8a) for the condition where the telemetry signal combiner has an assumed zero loss and the loss due to carrier tracking loop phase noise (radio loss) is negligible.

Up to this point, phase noise on the first local oscillator due to predetection carrier signal-to-noise power ratio has been examined. Total phase noise on the first local oscillator also includes phase noise from the local oscillator (VCO × Q) of receiving system 2 through N, which is coupled through the summing junction (as developed in Ref. 1). Consequently, the total phase noise at the output of the principal carrier tracking loop (i.e., on the first local oscillator) becomes

$$\left[\sigma^2_{\phi_{n1\Sigma 1,2}} + \left(\frac{\beta_2 \sigma_{\phi_{n2}}}{1 + \beta_2} \right)^2 \right]^{1/2} \tag{9}$$

for two receiving systems arrayed. For N receiving systems arrayed, the total rms phase noise on the first local oscillator is

$$\left[\sigma^2_{\phi_{n1\Sigma,\ldots,N}} + \left(\frac{\beta_2 \sigma_{\phi_{n2}}}{1 + \beta_2} \right)^2 + \cdots + \left(\frac{\beta_N \sigma_{\phi_{nN}}}{1 + \beta_N} \right)^2 \right]^{1/2} \tag{10}$$

As developed in Ref. 1, the total rms phase noise in expressions (9) and (10) can be considered as due to an equivalent predetection carrier signal-to-noise ratio within the closed-loop noise bandwidth of the RF carrier phase tracking loop. Comparison of this equivalent carrier signal-to-noise ratio in a single receiving system (i.e., system 1) provides the improvement due to radio frequency carrier arraying for the high-rate telemetry configuration where some portion of the predetection noise is not statistically independent among the various receiving systems of the array.

As described in Ref. 1, the RF carrier phase tracking loops in receiving systems 2 through N are also second-order loops which utilize a bandpass limiter and sinusoidal phase detector. Since the closed-loop noise bandwidth of the carrier phase tracking loop for receiving systems 2 through N is much narrower (by design) than that in receiving system 1, phase noise in receiving system 1 carrier tracking loop produces a reduction in predetection signal-to-noise ratio for receiving systems 2 through N. The resultant predetection carrier signal-to-noise ratio in receiving system 2 for two systems arrayed is then

$$\frac{P_{c2\Sigma 1,2}}{P_{n2}} = \frac{P_{c_2} \left(1 - \frac{\sigma^2_{\phi n1\Sigma 1,2}}{2} \right)^2}{NBW_{F_{A2}} \cdot N_{o2}} \tag{11}$$

which produces an rms phase noise

$$\sigma_{\phi_{n2\Sigma1,2}} = \frac{\frac{N_{o2}}{2} \cdot 2B_{L2}}{P_{c2\Sigma1,2}} \cdot \left[\frac{1 + \frac{P_{c2\Sigma1,2}}{NBW_{F_{A2}} \cdot N_{o2}}}{0.862 + \frac{P_{c2\Sigma1,2}}{NBW_{F_{A2}} \cdot N_{o2}}} \cdot \frac{\exp\left(\frac{N_{o2} \cdot B_{L2}}{P_{c2\Sigma1,2}}\right)}{\sinh\left(\frac{N_{o2} \cdot B_{L2}}{P_{c2\Sigma1,2}}\right)} \right]^{1/2} \text{rad, rms} \tag{12}$$

For N systems arrayed, the predetection carrier signal-to-noise ratio in receiving system 2 is

$$\frac{P_{c2\Sigma1,\ldots,N}}{P_{n2}} = \frac{P_{o2}\left(1 - \frac{\sigma^2_{\phi_{n1\Sigma1,\ldots,N}}}{2}\right)^2}{NBW_{F_{A2}} \cdot N_{o2}} \tag{13}$$

and the predetection carrier signal-to-noise ratio in receiving system N is

$$\frac{P_{cN\Sigma1,\ldots,N}}{P_{nN}} = \frac{P_{cN}\left(1 - \frac{\sigma^2_{\phi_{n1\Sigma,\ldots,N}}}{2}\right)^2}{NBW_{F_{AN}} \cdot N_{o_N}} \tag{14}$$

Substitution of corresponding terms from (13) or (14) into expression (12) provides $\sigma_{\phi_{n2\Sigma1,\ldots,N}}$ or $\sigma_{\phi_{N\Sigma1,\ldots,N}}$ for receiving system 2 or N respectively (Ref. 1). As noted previously (Ref. 1), the term $\sigma_{\phi_{n1\Sigma1,\ldots,N}}$ in expression (13) should be replaced by an rms value similar to that shown in expression (10) with the term $\beta_2\ \sigma_{\phi_{n2}}/(1 + \beta_2)$ deleted. This iteration results in a very small change in carrier signal-to-noise ratio improvement for the parameters considered here. A similar iteration applies to expression (14).

IV. Performance

Improvement in predetection signal-to-noise ratio can be determined from expressions (7a) and (8a) developed in Section III of this article. These expressions apply under the condition that in a predetection bandwidth which encompasses the signal of interest, the phase shift and group delay in the various receiving systems of the array are essentially matched. In addition, as outlined in Section III, the varying group delay on the telemetry sidebands is tracked out among the various receiving systems of the array by the telemetry signal combiner during a station pass. Also, for telemetry, the effective signal-to-noise ratio improvement obtained does not include the telemetry signal combiner loss and the loss (radio loss) due to carrier tracking loop phase noise (σ_{ϕ_n}).

Figure 2 shows the improvement in predetection signal-to-noise ratio as a function of the statistically independent portion of the predetection noise ($1 - \epsilon$) with two receiving systems arrayed for γ_2 values of 1.0, 0.95, 0.90, and 0.84 for the case where $\beta_2 = \gamma_2$. As defined in Section III, γ_2^2 is the carrier power-to-noise spectral density ratio of receiving system 2 relative to receiving system 1, and β_2 is the voltage coupling of receiving system 2 relative to receiving system 1 at the summing junction. Improvement in RF carrier predetection signal-to-noise ratio is maximum for $\beta = \gamma$ when the predetection noise is all statistically independent (noncoherent) or $1 - \epsilon = 1$, which is generally representative for the DSN. This maximum has a broad peak with variation of β about γ. Figure 2 also represents the effective telemetry signal-to-noise ratio improvement for the conditions described in the preceding paragraph for the case where the voltage coupling (β) = γ in the telemetry signal combining process. The resultant decrease in signal-to-noise ratio improvement is shown in Fig. 2 as an increasing portion of predetection noise (ϵ) becomes coherent or as the statistically independent portion of predetection noise ($1 - \epsilon$) decreases. Figures 3, 4, and 5 show similar characteristics for three, four, and six similar receiving systems arrayed. Figures 6, 7 and 8 show the effect on predetection signal-to-noise ratio improvement with γ values of 1.0, 0.95, 0.90 and 0.84 for two, three and four receiving systems arrayed,

respectively, when the summing junction voltage coupling β is varied. Also shown in Figs. 6, 7, and 8 is the effect on predetection signal-to-noise ratio improvement when the portion of predetection noise that is statistically independent is 1.0, 0.8 or 0.5.

Consider next the equivalent RF carrier signal-to-noise ratio improvement as determined from the total rsm phase noise on the first local oscillator (see expressions 9 and 10 and associated discussion in Section III). The following sets of design parameters apply for the performance presented in this report. The sets of parameters for receiving system 1 are:

Threshold two-sided noise bandwidth $2B_{L_{01}}$	12	152	30 Hz
Predetection IF filter noise bandwidth $NBW_{F_{A1}}$	2200	2200	2000 Hz
while the corresponding sets of parameters for receiving system 2 through N are:			
Threshold two-sided noise bandwidth $2B_{L_{02,\ldots,N}}$	0.1	1.0	0.3 Hz
Predetection IF filter noise bandwidth $NBW_{F_{A2,\ldots,N}}$	2200	2200	2000 Hz

Using the parameters above, Fig. 9 shows the equivalent RF carrier signal-to-noise ratio improvement for two similar receiving systems arrayed (high-rate telemetry configuration) as a function of summing junction voltage coupling β_2. Performance is shown for γ_2 values of 1.0, 0.95, 0.90, and 0.84 with $1 - \epsilon$ values of 1.0, 0.8, and 0.5. Performance for $1 - \epsilon = 1$ represents the same as that shown in Fig. 3 (Ref. 1) for two systems. Note that, in general, performance variation with voltage coupling β_2 is quite gradual. The information shown in Fig. 9 can be rearranged to show RF carrier signal-to-noise ratio improvement as a function of $1 - \epsilon$. Figures 10a and 10b show this characteristic for two similar systems arrayed for the same values of γ_2 as in Fig. 9, with voltage coupling values of 1.0 and 0.5, respectively.

Equivalent RF carrier signal-to-noise ratio improvement for three similar receiving systems arrayed (as determined from total rms phase noise on the first local oscillator) is shown in Figs. 11, 12a, and 12b as a function of voltage coupling and $1 - \epsilon$, respectively. Similar characteristics are shown in Figs. 13, 14a and 14b for four similar receiving systems arrayed while Figs. 15, 16a, and 16b apply to six similar receiving systems arrayed.

Some initial measurements of radio-frequency carrier signal-to-noise ratio improvement have been made in the laboratory for two and three receiving systems arrayed. These initial measurements were made with one of the sets of parameters described above. In particular, the predetection IF filter noise bandwidth was 2200 Hz with a $2B_{Lo}$ of 152 Hz for receiving system 1 and a $2B_{Lo}$ of 1 Hz for receiving systems 2 and 3. Measurement with two receiving systems arrayed with $1 - \epsilon_2$ and γ_2 equal to 1 provided an RF carrier signal-to-noise ratio improvement of 2.8 dB for $\beta_2 = 1$, an improvement of 2.4 dB for $\beta_2 = 0.5$, and an improvement of 2.5 dB for $\beta_2 = 1.0$ and $\gamma_2 = 0.94$. The corresponding calculated improvement is 2.9, 2.5 and 2.6 dB respectively. Measurement with $1 - \epsilon_2 = 0.75$ and $\gamma_2 = \beta_2 = 1$ provided a 2.0-dB RF carrier signal-to-noise ratio improvement. An improvement of 1.8 dB was measured for $1 - \epsilon = 0.77$ with $\gamma_2 = 1$ and $\beta_2 = 0.5$. These values agree with predicted performance (see Figs. 9, 10a, and 10b).

Measurement with three receiving systems arrayed with $(1 - \epsilon_2) = (1 - \epsilon_3) = 1$ and $\beta_2 = \beta_3 = 1$ provided an RF carrier signal-to-noise ratio improvement of 4.3 dB for $\gamma_2 = \gamma_3 - 1$ and an improvement of 4 dB for $\gamma_2 = 0.94$ and $\gamma_3 = 0.93$, which agree with predicted performance (see Fig. 11). Measurement with $(1 - \epsilon_2) = (1 - \epsilon_3) = 0.77$ and $\gamma_2 = \gamma_3 = 1$ provided an RF carrier signal-to-noise ratio improvement of 2.7 dB with $\beta_2 = \beta_3 = 1$ and also with $\beta_2 = \beta_3 = 0.5$. These values agree with predicted performance (see Figs. 12a and 12b).

V. Discussion

The following material examines the situation where a planet in the solar system is within the beamwidth of the array considered in this report.

Consider the case of two receiving systems (1 and 2) arrayed for coherent reception of a signal from a spacecraft at planetary distance. A planet in the solar system is within the beamwidth of the two antennas of the array. This two-aperture (antenna) array will see the hot body (noise) radiation from the planet as an interferometer operating at a reception frequency wavelength λ. Designate the effective distance between the antennas of two stations as $B_{1,2}$ with $B_{r_{1,2}}$ as the component that is perpendicular to the line of sight to the planet. The fringe spacing of the interferometer is then $\lambda/B_{r_{1,2}}$ radians.

Consider for the moment, a situation where the planet appears as a point noise source. That is, the angular size of the planet as seen from Earth is very small compared to the fringe spacing ($\lambda/B_{r_{1,2}}$). Within the fringe spacing (as the Earth rotates), the noise radiation from the planet as seen in the predetection bandwidth of the array is in phase for the two receivers at the center of an angular segment $\lambda/2B_{r_{1,2}}$, orthogonal at each edge of the angular segment, and 180° out of phase at the center of the adjacent angular segments $\lambda/2B_{r_{1,2}}$ due to continuing change in path length to the two antennas. This in-phase/out-of-phase situation continues alternately during a station pass as the array tracks the spacecraft and it is superimposed on the statistically independent portion of predetection noise. For this situation of a planet appearing as a point noise source and representing a given fractional part (ϵ) of operating equivalent system noise temperature (T_{op}), the decrease in predetection signal-to-noise ratio improvement shown in Fig. 2 (for the corresponding $(1 - \epsilon)$) corresponds to the in-phase predetection noise condition at the center of an angular segment $\lambda/2B_{r_{1,2}}$. The orthogonal predetection point noise source condition corresponds to a signal-to-noise ratio improvement for $(1 - \epsilon) = 1$, while the 180° out-of-phase point noise source condition essentially provides signal-to-noise ratio improvement for $(1 - \epsilon) = 1$, but at a T_{op} without the point noise source contribution. The discussion above also applies to RF carrier signal-to-noise ratio improvement as shown in Figs. 9, 10a, and 10b for two similar receiving systems arrayed.

A planet of the solar system may not appear as a point noise source for the array considered here. In fact, it can have an angular size that is larger than the fringe spacing $\lambda/B_{r_{1,2}}$. The following development addresses this consideration. In general for the application presented in this report, the planets (as viewed from Earth) can be characterized as disks with a uniform brightness distribution D at the reception frequency. The brightness distribution will be a function of the reception frequency. Utilizing information in Ref. 3 and writing the brightness transform as a function of the angular size (ν) of the planet and the inverse of fringe spacing, the brightness transform R becomes

$$R_{1,2} = \frac{1}{\nu}\int_{-\nu/2}^{+\nu/2} D(\omega) e^{-2\pi i\left(\frac{B_{r_{1,2}}}{\lambda}\right)\chi}\, d\chi \tag{15}$$

with integration from the centerpoint of the planet disk out to the edges. Integration of expression (15) provides

$$R_{1,2} = D(\omega) \cdot \frac{\sin\left(\pi \frac{B_{r_{1,2}}}{\lambda}\nu\right)}{\pi \frac{B_{r_{1,2}}}{\lambda}\nu} \tag{16}$$

For the situation where the planet appears as a point noise source, the sin x/x type of expression above approaches one. The brightness transform becomes the total power of the noise source (planet) as seen in the predetection bandwidth and the preceding discussion relating to a point noise source applies. Figure 17 shows expression (16) plotted as a function of the ratio of planet angular size to fringe spacing $[\nu/(\lambda/B_{r_{1,2}})]$. Note that the above integral is centered ($\nu = 0$) on the in-phase predetection noise situation at the center of an angular segment $\lambda/2B_{r_{1,2}}$ that was discussed earlier in this section of the report. Figure 17 is the resultant amplitude of the brightness transform for this particular path length situation to the two antennas for various ratios of planet angular size to fringe spacing. This figure shows the magnitude of the correlated portion of noise power relative to total

noise power from the planet which is defined as fringe visibility for radio interferometry measurements (Ref. 3). Consequently Fig. 17 provides the information necessary to scale the coherent portion of predetection noise relative to a point noise source for any ratio of planet angular size to fringe spacing $[\nu/(\lambda/B_{r_{1,2}})]$. Any point on Fig. 17 can be treated as an equivalent reduced-in-magnitude point noise source representing a reduced ϵ, and the resulting reduction in predetection and RF carrier signal-to-noise ratio improvement can be determined from Figs. 2, 9, 10a and 10b.

Consider next three receiving systems (1, 2 and 3) arrayed for coherent reception of a spacecraft signal with a planet within the beamwidth of the three antennas. For the moment, consider a situation where the planet appears as a point noise source which represents a given fractional part (ϵ) of the operating equivalent system noise temperature (T_{op}). At those times when the noise radiation from the planet as seen in the predetection bandwidth of the array is in-phase from receivers 1 and 3 in an angular segment $\lambda/2B_{r_{1,3}}$ at essentially the same time as it is from receivers 1 and 2 in an angular segment $\lambda/2B_{r_{1,2}}$, the decrease in predetection signal-to-noise ratio improvement shown in Fig. 3 applies for the corresponding $(1 - \epsilon)$ value. At all other times, the decrease in predetection signal-to-noise ratio improvement will be less. This discussion also applies to RF carrier signal-to-noise ratio improvement shown in Figs. 11, 12a, and 12b for three similar systems arrayed.

For the situation where the planet is not a point source, the normalized brightness transforms for three receiving systems become

$$R_{1,2,3} = \frac{D(\omega)}{2}\left(\frac{\sin\left(\pi \frac{B_{r_{1,2}}}{\lambda}\nu\right)}{\pi \frac{B_{r_{1,2}}}{\lambda}\nu} + \frac{\sin\left(\pi \frac{B_{r_{1,3}}}{\lambda}\nu\right)}{\pi \frac{B_{r_{1,3}}}{\lambda}\nu}\right) \tag{17}$$

Note again in this case, the above expression (17) represents a result centered ($\nu = 0$) on the in-phase predetection noise situation at the center of angular segment $\lambda/2B_{r_{1,2}}$ and simultaneously at the center of angular segment $\lambda/2B_{r_{1,3}}$. For this particular path length situation and given fringe spacings $\lambda/B_{r_{1,2}}$ and $\lambda/B_{r_{1,3}}$, expression (17) can be evaluated and the effect of the planet on decrease in predetection and RF signal-to-noise ratio improvement can be determined from Figs. 3, 11, 12a, and 12b. Extension of the above discussion can be applied to four or more similar receiving systems arrayed.

To illustrate the above, consider a 300-meter $B_{r_{1,2}}$ between two stations arrayed (34-meter-diameter antennas) and operating at a reception frequency of 8420 MHz ($\lambda = 3.56$ cm). The resultant fringe spacing is 24.5 arcsec. The planet Venus is in the beamwidth of the antennas, its contribution to system noise temperature is 10 kelvins and it subtends an angle of 42. arcsec. The ratio 42./24.5 equals 1.7 which, from Fig. 17, provides a reduction in relative magnitude of correlated noise power to 0.125 or 1.25 kelvins. The operating system temperature is 20 + 10 = 30 kelvins. The statistically independent portion $(1 - \epsilon)$ of predetection noise power is (30 - 1.25)/30 or 0.958. Reduction in predetection and RF carrier signal-to-noise ratio improvement is 0.16 dB (Figs. 2 and 10a) at those times during a station pass when the fractional noise (0.125) from Venus is in-phase in the predetection bandwidth of the two arrayed receiving systems. Note that if the 10 kelvins represented a point noise source, reduction in signal-to-noise ratio improvement would be 1.2 dB instead of 0.16 dB since $1 - \epsilon$ becomes (30 - 10)/30 or 0.667.

References

1. Brockman, M. H., "Radio Frequency Carrier Arraying for High Rate Telemetry," in *The Deep Space Network Progress Report 42-45*, pp. 209-223, Jet Propulsion Laboratory, Pasadena, Calif., June 15, 1978.

2. Brockman, M. H., "Radio Frequency Carrier Arraying for Near Maximum Carrier Signal-to-Noise Ratio Improvement," in *The Deep Space Network Progress Report 42-49*, pp. 99-106, Jet Propulsion Laboratory, Pasadena, Calif., Feb. 15, 1979.

3. Thomas, J. B., An Analysis of Source Structure Effects in Radio Interferometry Measurements, Publication 80-84, Jet Propulsion Laboratory, Pasadena, Calif., Dec. 15, 1980.

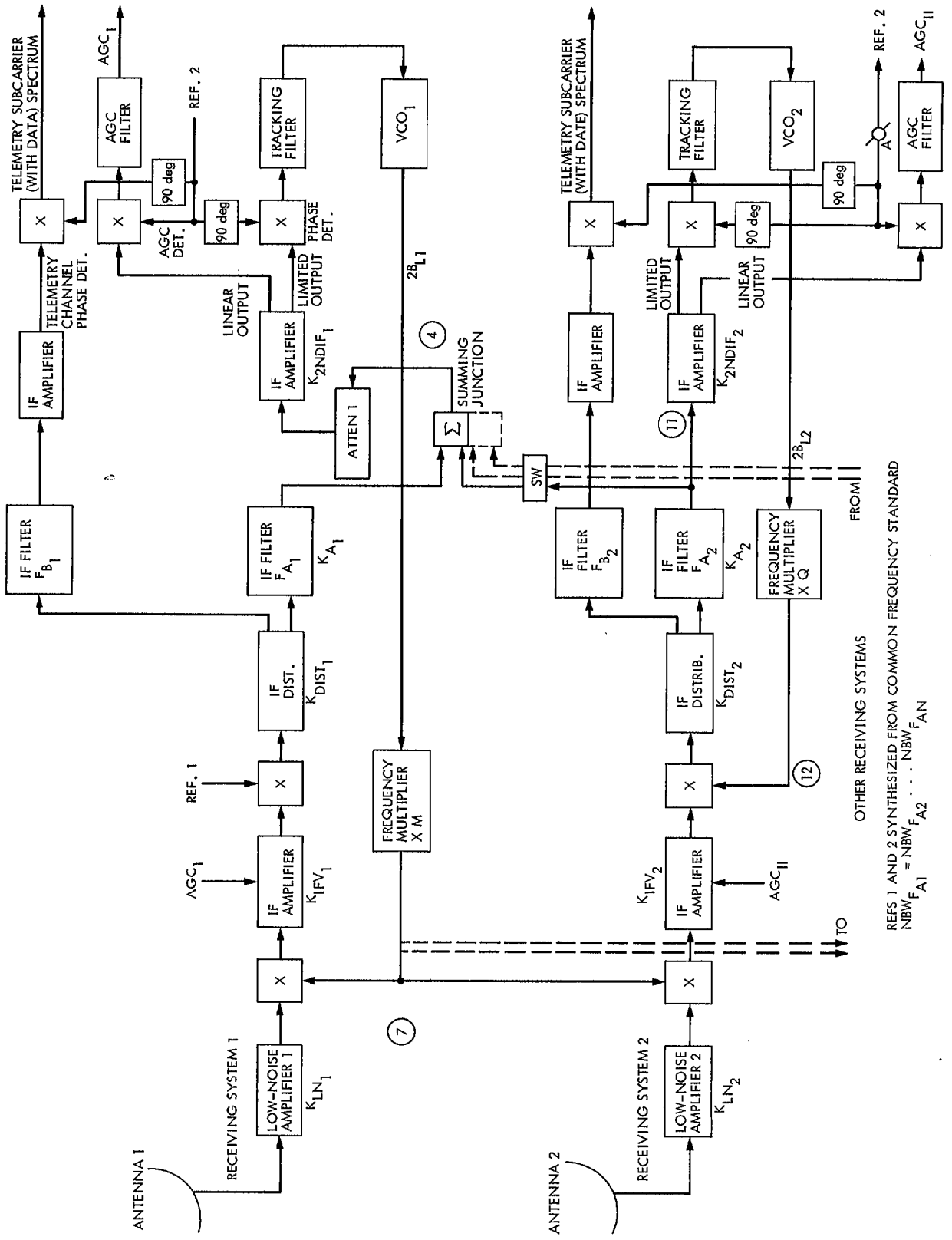

Fig. 1. Radio frequency carrier arraying for high-rate telemetry reception

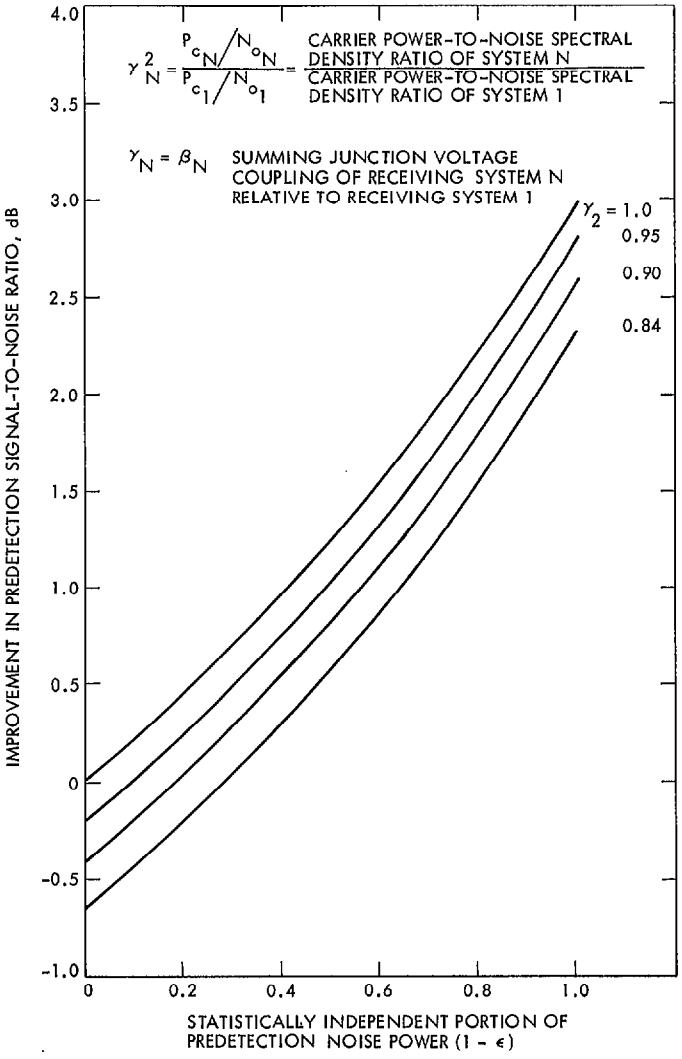

Fig. 2. Effect of partial coherence in system noise temperature on predetection signal-to-noise ratio improvement, two receiving systems arrayed

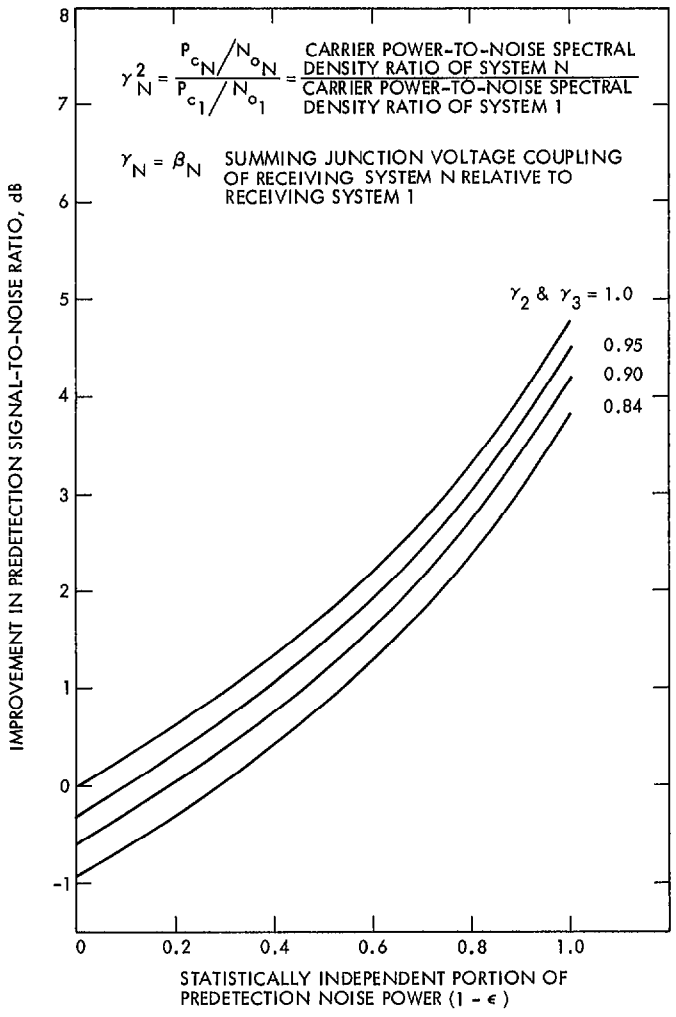

Fig. 3. Effect of partial coherence in system noise temperature on predetection signal-to-noise ratio improvement, three receiving systems arrayed

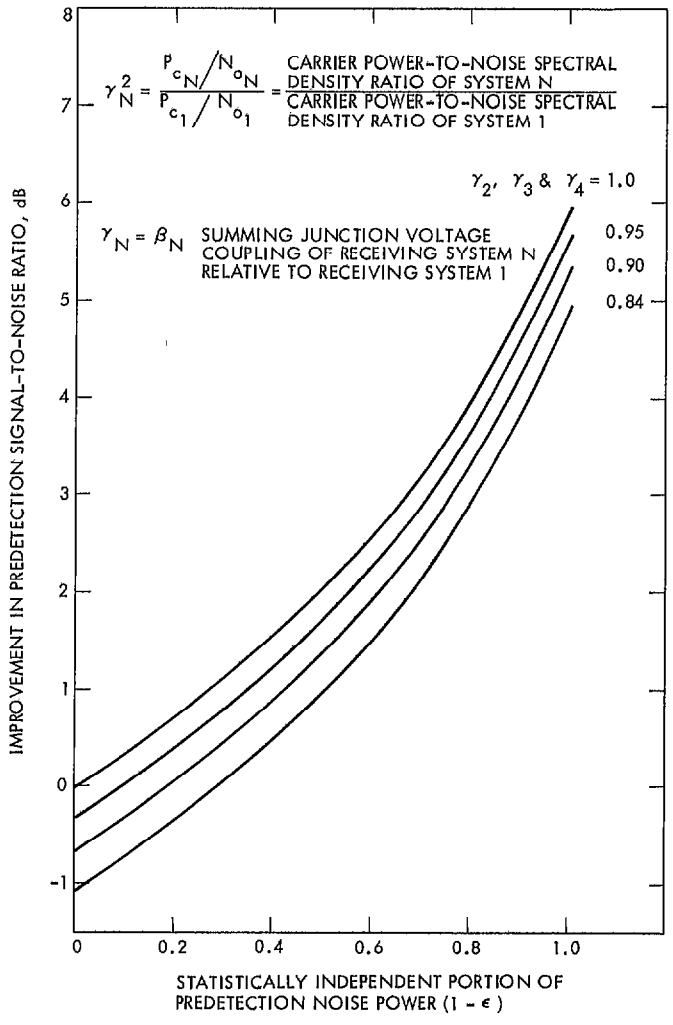

Fig. 4. Effect of partial coherence in system noise temperature on predetection signal-to-noise ratio improvement, four receiving systems arrayed

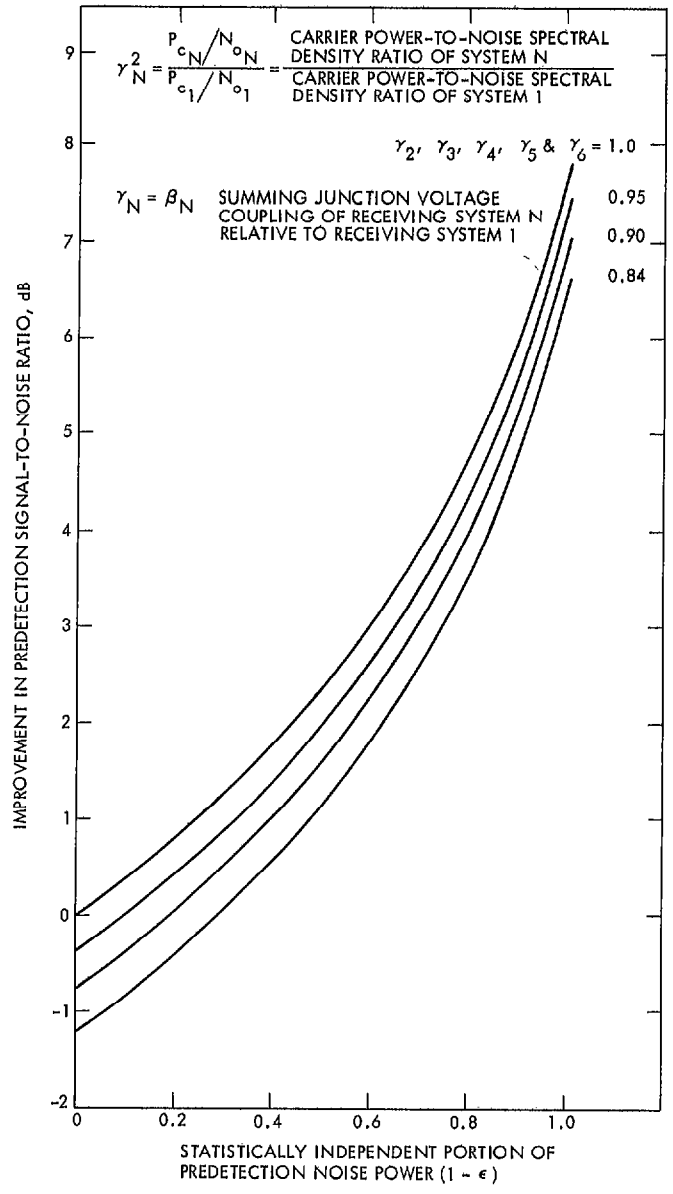

Fig. 5. Effect of partial coherence in system noise temperature on predetection signal-to-noise ratio improvement, six receiving systems arrayed

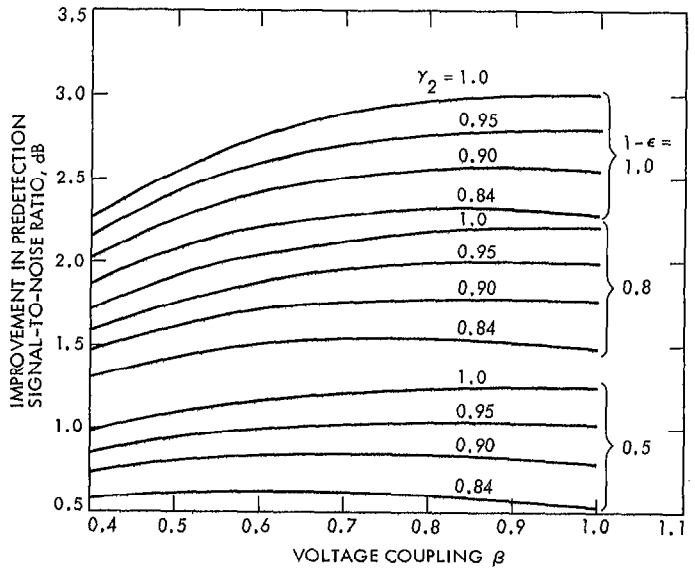

Fig. 6. Effect of summing junction voltage coupling on predetection signal-to-noise ratio improvement with partial coherence in system noise temperature, two receiving systems arrayed

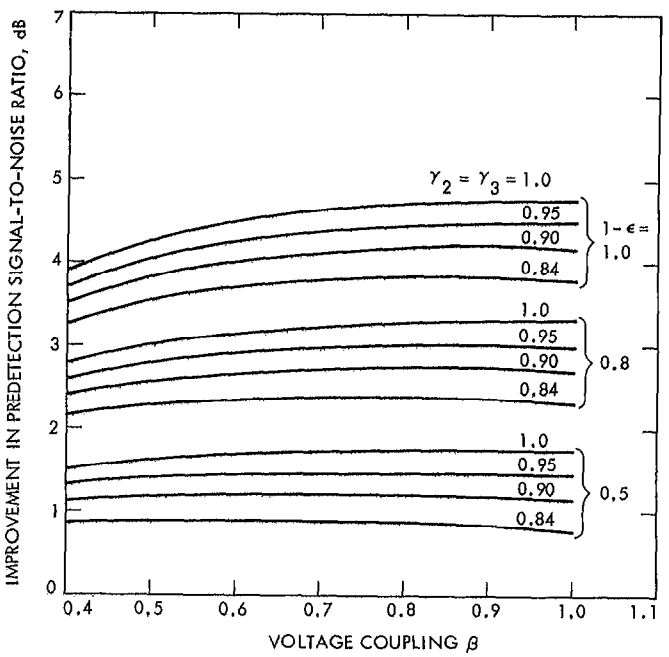

Fig. 7. Effect of summing junction voltage coupling on predetection signal-to-noise ratio improvement with partial coherence in system noise temperature, three receiving systems arrayed

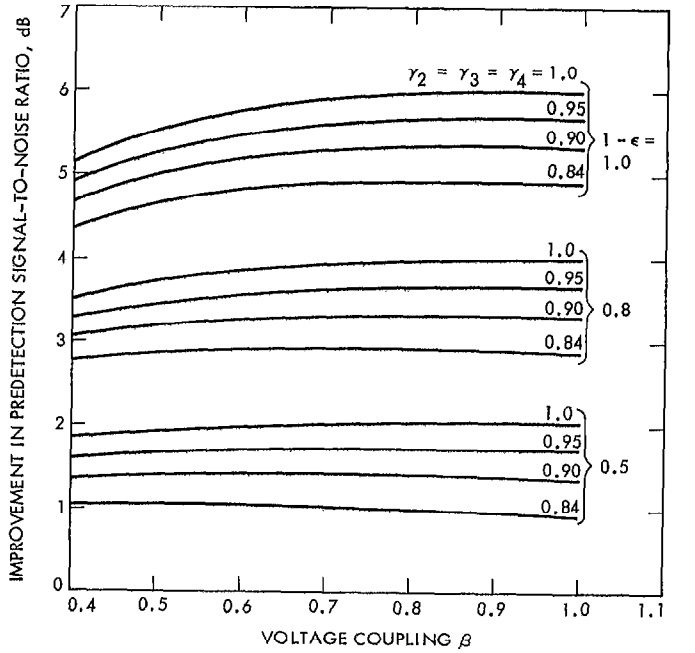

Fig. 8. Effect of summing function voltage coupling on predetection signal-to-noise ratio improvement with partial coherence in system noise temperature, four receiving systems arrayed

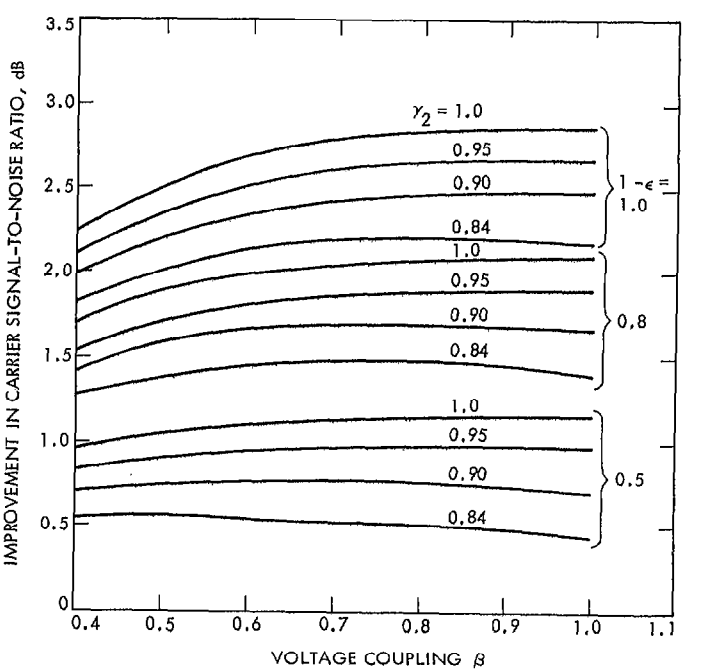

Fig. 9. Effect of summing junction voltage coupling on carrier signal-to-noise ratio improvement with partial coherence in system noise temperature, two receiving systems arrayed, high-rate telemetry configuration

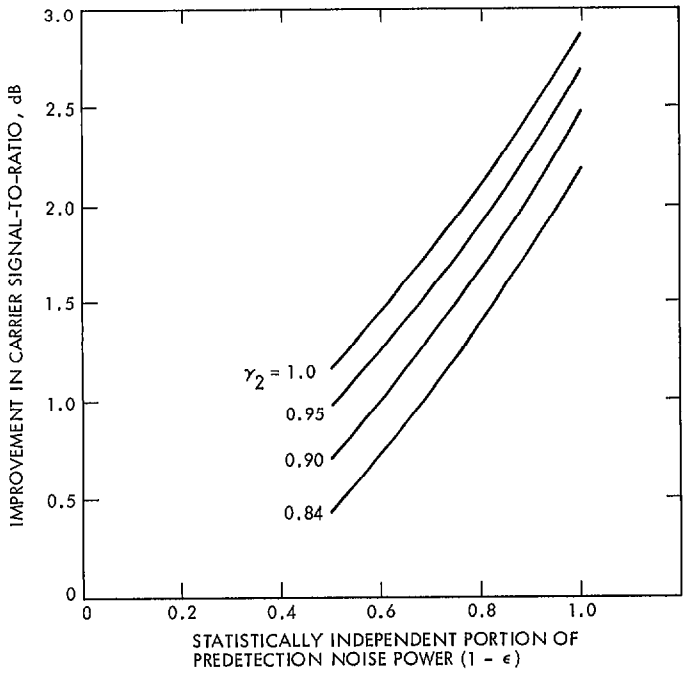

Fig. 10a. Effect of partial coherence in system noise temperature on carrier signal-to-noise ratio improvement, two receiving systems arrayed, high-rate telemetry configuration, voltage coupling $\beta = 1$

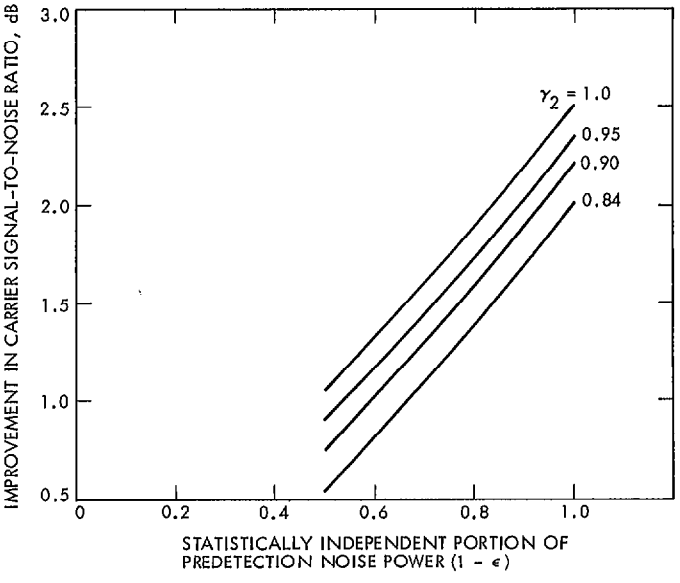

Fig. 10b. Effect of partial coherence in system noise temperature in carrier signal-to-noise ratio improvement, two receiving systems arrayed, high-rate telemetry configuration, voltage coupling $\beta = 0.5$

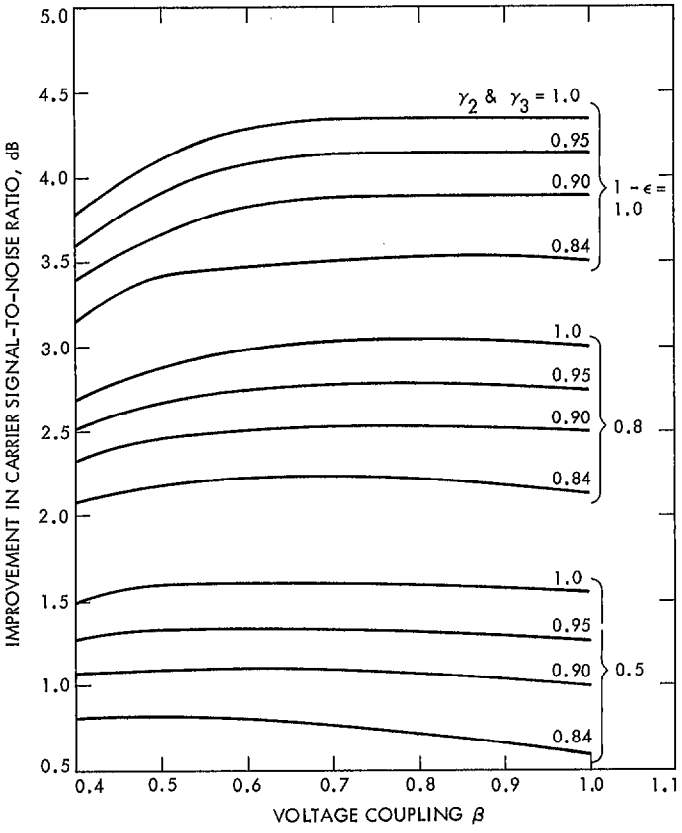

Fig. 11. Effect of summing junction voltage coupling on carrier signal-to-noise ratio improvement with partial coherence in system noise temperature, three receiving systems arrayed, high-rate telemetry configuration

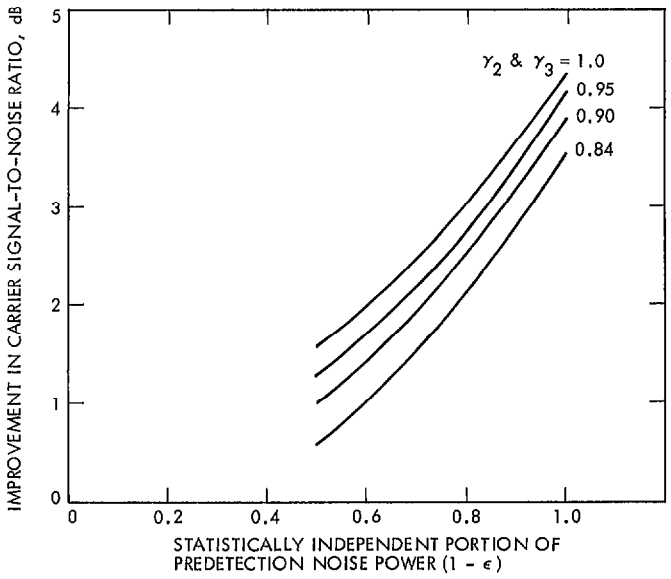

Fig. 12a. Effect of partial coherence in system noise temperature on carrier signal-to-noise ratio improvement, three receiving systems arrayed, high-rate telemetry configuration, voltage coupling $\beta = 1$

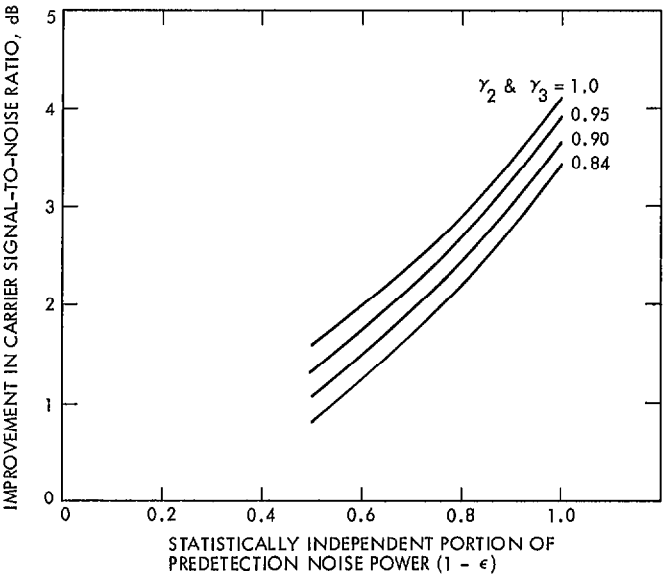

Fig. 12b. Effect of partial coherence in system noise temperature in carrier signal-to-noise ratio improvement, three receiving systems arrayed, high-rate telemetry configuration, voltage coupling $\beta = 0.5$

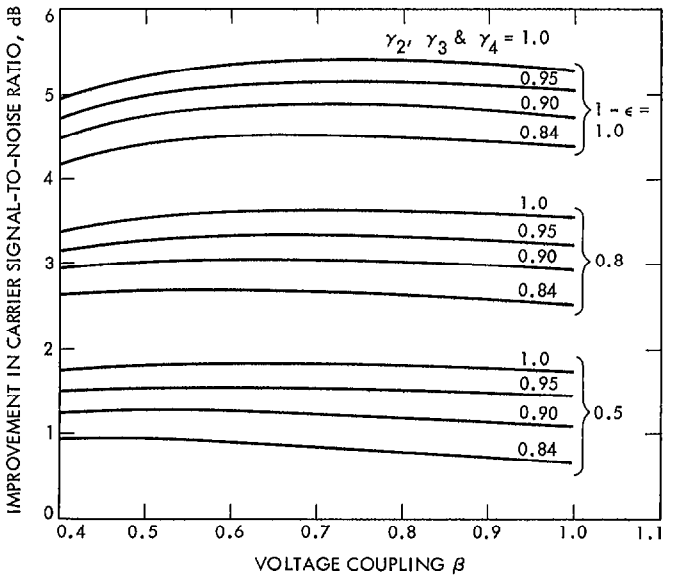

Fig. 13. Effect of summing junction voltage coupling on carrier signal-to-noise ratio improvement with partial coherence in system noise temperature, four receiving systems arrayed, high-rate telemetry configuration

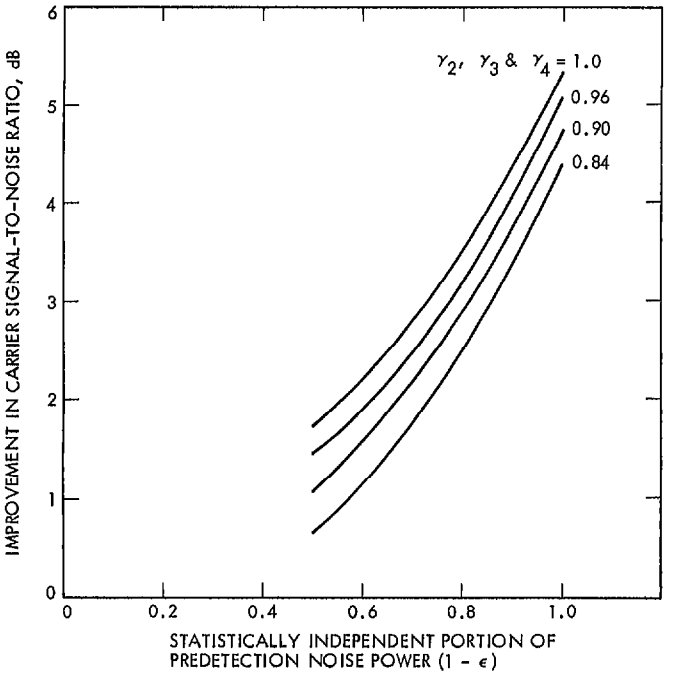

Fig. 14a. Effect of partial coherence in system noise temperature on carrier signal-to-noise ratio improvement, four receiving systems arrayed, high-rate telemetry configuration, voltage coupling $\beta = 1$

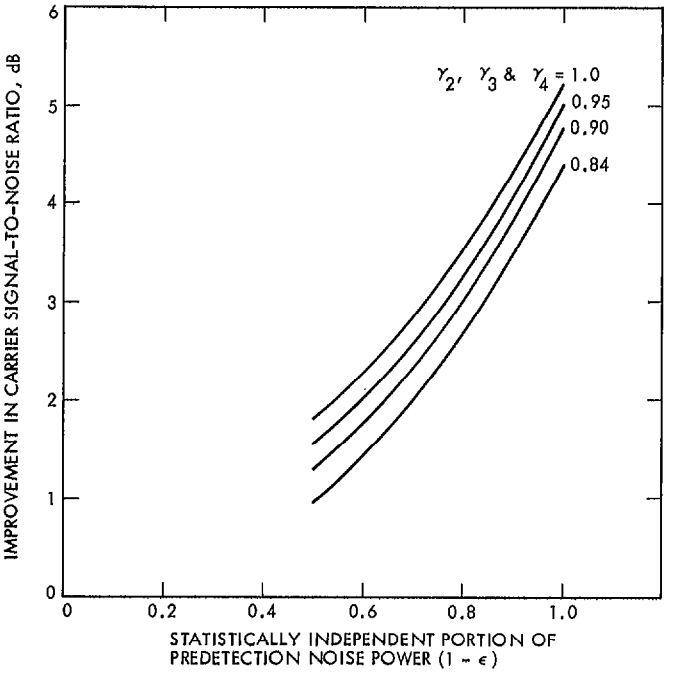

Fig. 14b. Effect of partial coherence in system noise temperature on carrier signal-to-noise ratio improvement, four receiving systems arrayed, high-rate telemetry configuration, voltage coupling $\beta = 0.5$

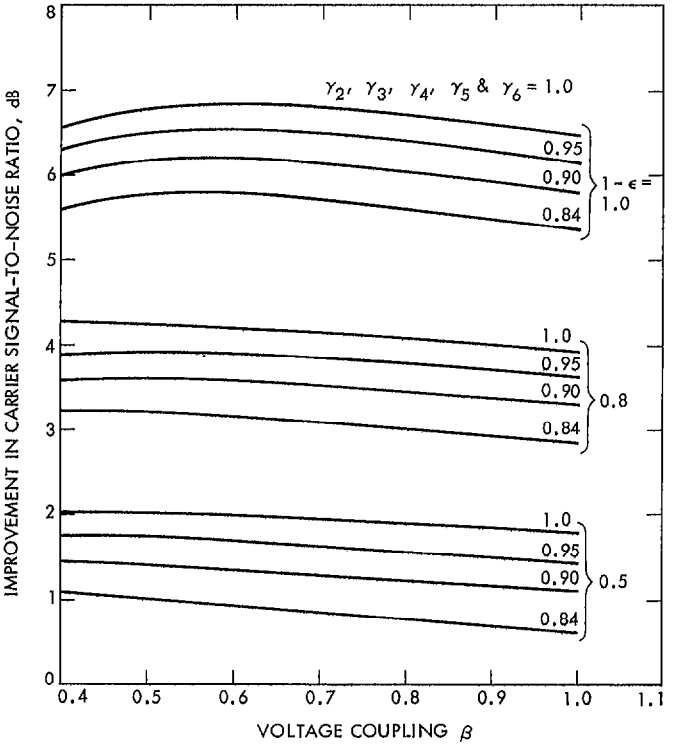

Fig. 15. Effect of summing junction voltage coupling on carrier signal-to-noise ratio improvement with partial coherence in system noise temperature, six receiving systems arrayed, high-rate telemetry configuration

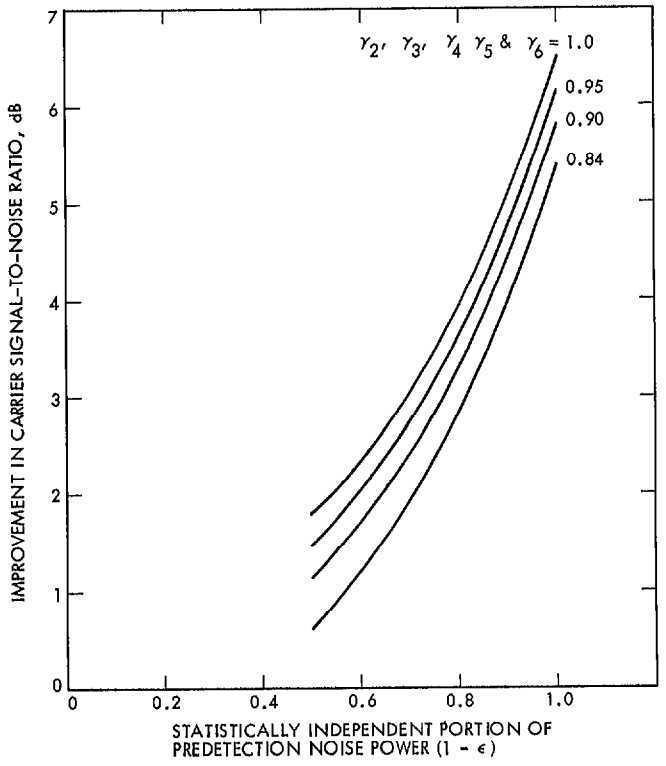

Fig. 16a. Effect of partial coherence in system noise temperature on carrier signal-to-noise ratio improvement, six receiving systems arrayed, high-rate telemetry configuration, voltage coupling $\beta = 1$

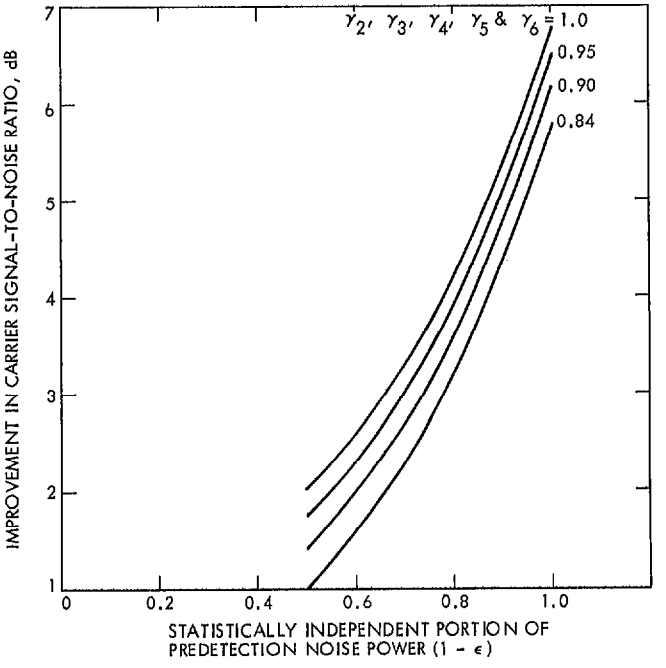

Fig. 16b. Effect of partial coherence in system noise temperature on carrier signal-to-noise ratio improvement, six receiving systems arrayed, high-rate telemetry configuration, voltage coupling $\beta = 0.5$

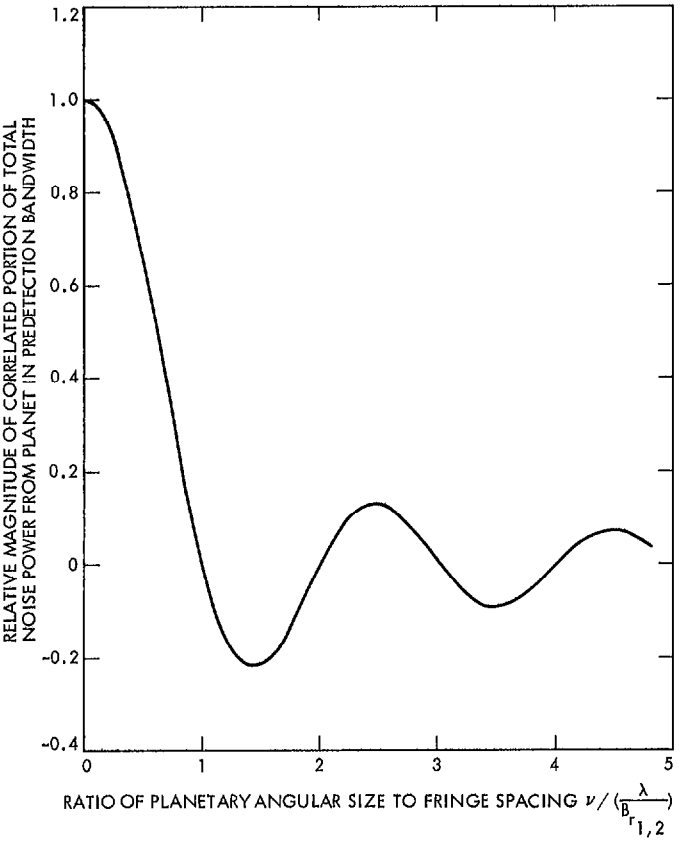

Fig. 17. Relative effect of ratio of planet angular size to fringe spacing on correlated predetection noise, two antenna array